Laser and Particle Beams (2002), *20*, 13–21. Printed in the USA.

DOI: 10.1017.S0263034602201020

Rapid fuel layering inside moving free-standing ICF targets: Physical model and simulation code development

I.V. ALEKSANDROVA,[1] S.V. BAZDENKOV,[1] AND V.I. CHTCHERBAKOV[2]

[1]P.N. Lebedev Physical Institute, Russian Academy of Sciences, P.O. Box 117924, Leninskiy prospect 53, Moscow, Russia
[2]Moscow State University, Department of Low Temperatures Physics, P.O. Box 119899, Vorobijovy Gory 4, Moscow, Russia

(RECEIVED 26 April 2001; ACCEPTED 23 October 2001)

Abstract

In this report, we discuss the physical concept and the results of mathematical modeling of free-standing target (FST) layering for inertial confinement fusion (ICF), including the detailed descriptions of the heat transfer and layer symmetrization mechanisms.

Keywords: Free standing target; Inertial confinement fusion; Self-symmetrization

1. INTRODUCTION

A prototype of the system for mass-producing cryogenic targets has been created at the Lebedev Physical Institute (LPI). The system is capable of filling, layering, and delivering large, free-standing (unmounted) cryogenic targets. This allows one to carry out the experiments on rapid formation and self-symmetrization of a fuel layer onto the inner surface of a spherical shell. The observed layering time does not exceed 12 s for H_2 and D_2 layers. The cryogenic targets for these experiments are polystyrene shells of 0.7- to 1-mm diameter and 8- to 15-μm wall thickness. The layer thickness is between 30 and 100 μm. The FST system operates with 25 targets at one time. They remain unmounted in each production step. The transport process is target injection between fundamental system elements: shell container—layering module—test chamber (see Fig. 1).

Most of the theoretical effort has focused on development of mathematical models which describe each production step in the FST system: rapid filling to decrease the radiation damage due to β-ray from tritium decay during the diffusion fill (Aleksandrova & Belolipetskiy, 1999*a*, 1999*b*), rapid layering to fabricate the homogeneous fuel (Aleksandrova *et al*., 1993, 1994, 1996*b*, 2000*b*), rapid target characterization (Aleksandrova *et al*., 1999*b*, 2000*a*), and delivery (Koresheva *et al*., 1994; Aleksandrova *et al*., 1999*a*, 1996*a*) to ensure the layer quality survival. In this work we present new results relative to cryogenic solid layering (Aleksandrova *et al*., 2001).

2. SIMULATION CODE FOR RAPID FUEL LAYERING INSIDE MOVING FREE-STANDING ICF TARGETS

Modeling the FST layering was aimed at determination of a prevailing layering mechanism and development of a baseline program for calculation of a corresponding layering time. The heat transfer mechanism is a key moment in cryogenic layer formation. In the experiment, the fuel cooling and the phase transitions in the shell are inevitably three-dimensional (3D) processes because, in principle, it is vital to avoid unwanted side effects: nonspherical heat removal from the target, a nonradial temperature gradient, and gravitational sag of the liquid fuel. Thus, the correct mathematical descriptions of the fuel layering require 3D model development. However, these effects play only quantitative role and can change the value of τ_{form} several times, whereas there is a physically important parameter which qualitatively changes τ_{form} several orders of magnitude. We mean the rate of heat removal from the target, that is, a thermal boundary condition onto the outer shell surface. Therefore, in estimating the role of heat transfer mechanism, one can use a one-dimensional spherically symmetric model as a first approximation for calculating the layering time τ_{form}.

Address correspondence and reprint requests to: I.V. Aleksandrova, P.N. Lebedev Physical Institute, Russian Academy of Sciences, P.O. Box 117924, Leninskiy prospect 53, Moscow, Russia.

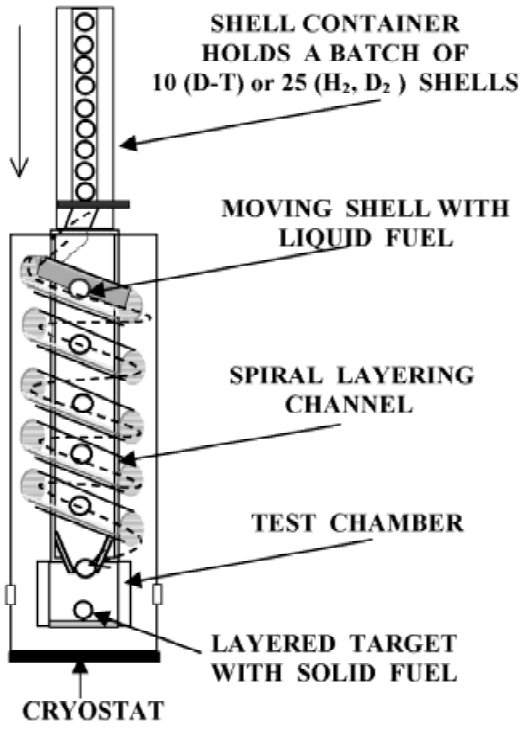

Fig. 1. Schematic of the layering module operation for a rep-rate cryogenic target fabrication.

The heat transfer in a one-dimensional spherically symmetrical model is described by the following equation:

$$\rho_l C_l \frac{\partial T_l}{\partial t} = \frac{1}{r^2}\frac{\partial}{\partial r}\left(r^2 k_l \frac{\partial T_l}{\partial r}\right) \tag{1}$$

for each fuel phase: gaseous ($l = gas$), liquid ($l = liquid$), solid ($l = solid$) and the shell ($l = sh$). The temperature $T_l(r)$ is continuous at boundaries between the fuel phases and the inner shell surface. Here we use the following nomenclature: ρ_l is the density, C_l is the heat capacity, k_l is the thermal conductivity, t is the current time.

The gas density ρ and the pressure P are related by the following equation:

$$P = \frac{R_g T}{(\mu_f/\rho) - b} - \frac{a\rho^2}{(\mu_f)^2}. \tag{2}$$

In Eq. (2) R_g is the gas constant, μ_f is the molecular weight, T is the absolute temperature, a and b are the temperature-dependent parameters. The gas mass in the target is known:

$$m_{gas}(t) \equiv \int_0^{r_{gl}} \rho_{gas}(T)\cdot 4\pi r^2\, dr, \tag{3}$$

where $r_{gl}(t)$ is the gas–liquid boundary. It can change in time due to phase transitions. The mass of the liquid and solid phases,

$$m_{liquid}(t) \equiv \int_{r_{gl}}^{r_{ls}} \rho_{liquid}(T)\cdot 4\pi r^2\, dr, \tag{4}$$

$$m_{solid}(t) \equiv \int_{r_{1g}}^{R} \rho_{solid}(T)\cdot 4\pi r^2\, dr, \tag{5}$$

serve for determination of the phase boundaries location: gas–liquid ($r = r_{gl}(t)$), and liquid–solid ($r = r_{ls}(t)$). The values of $m_{gas}(t)$, $m_{liquid}(t)$, $m_{solid}(t)$ can be found from the conditions of phase transitions at the fuel phase boundaries (Stephen's problem):

$$\lambda_{gl}(T_{gl})\cdot\frac{dm_{gas}}{dt} = -4\pi r_{gl}^2\left(\left[k_{gas}\frac{\partial T}{\partial r}\right]_{r=r_{gl}} - \left[k_{liquid}\frac{\partial T}{\partial r}\right]_{r=r_{gl}}\right), \tag{6}$$

$$\lambda_{ls}(T_{ls})\cdot\frac{dm_{solid}}{dt} = 4\pi r_{ls}^2\left(\left[k_{solid}\frac{\partial T}{\partial r}\right]_{r=r_{ls}} - \left[k_{liquid}\frac{\partial T}{\partial r}\right]_{r=r_{ls}}\right). \tag{7}$$

Here $\lambda_{gl}(T)$ and $\lambda_{ls}(T)$ are the phase transition heat, and $T_{gl} \equiv T|_{r=r_{gl}}, T_{ls} \equiv T|_{r=r_{ls}}$ are the temperatures at the fuel phase boundaries. Equations (6) and (7) should be added with the law of mass conservation:

$$\frac{d}{dt}\left(m_{gas} + m_{liquid} + m_{solid}\right) = 0. \tag{8}$$

The flow continuity at $r = R$, where R is the inner shell radius, is of the form

$$\left[k_l\frac{\partial T_l}{\partial r}\right]_{r=R} = \left[k_{sh}\frac{\partial T_{sh}}{\partial r}\right]_{r=R}. \tag{9}$$

In Eq. (9) subscript l corresponds the fuel phase which is located on the inner shell surface at a given time moment.

The boundary condition at the target center is evident:

$$\left[\frac{\partial T}{\partial r}\right]_{r=0} = 0. \tag{10}$$

The boundary condition at $r = R + \delta R$, where δR is the shell thickness, should be chosen from the experimental conditions. Three cases are thinkable in this respect.

2.1. High cooling rates; motionless target

To obtain high cooling rates, the target should be in thermal contact with an external agent. Such an agent, for example, can be liquid helium immediately surrounding the target. If the target is placed into a cryostat with a given temperature $T_{external}(t)$, then the boundary condition at $r = R + \delta R$ is of the form

$$T_{sh}(r = (1+\delta)R) = T_{externfl}(t). \tag{11}$$

https://doi.org/10.1017/S0263034602201020 Published online by Cambridge University Press

Table 1. *Comparative data for the glass and polystyrene shell; $\tau_{surface} = 1$ ms, $\delta R = 10$ μm*

	Glass				Polystyrene	
Gas	τ_1	τ_2	τ_3	τ_4	τ_1	τ_2
H_2 (25 mg/cc)	4.3	8.53	8.53	13.7	95.62	168.2
D_2 (50 mg/cc)	5.74	7.99	13.29	16.3	124.57	227.6

The modeling results are most conveniently analyzed by introducing the following parameters: $\tau_{surface}$ is the time (in milliseconds) of temperature drop at the outer shell surface, which is only dependent on the experimental conditions; $\tau_1, \tau_2, \tau_3, \tau_4$ (in milliseconds) are the times of the onset and the end of fuel liquefaction and freezing, respectively, and T_{in} is the target temperature before layering.

In the case of high cooling rates, the time of target cooling and solid layer formation are controlled by their own times of the heat transport in the fuel and the shell, τ_{gas} and τ_{shell}. The dynamics of fuel liquefaction and freezing is given in Table 1. In our calculations, the shell ($2R = 1$ mm, $\delta R = 10$ μm) is filled with hydrogen ($\rho = 25$ mg/cc) or deuterium ($\rho = 50$ mg/cc), $T_{in} = 300$ K, $\tau_{surface} = 1$ ms, unless otherwise specified. The shell material is glass or polystyrene.

Analyzing the layering processes in a motionless target, one should take into account the following characteristic parameters: the time of gravitational fuel sag to the target bottom and the time of liquid phase existence.

The characteristic time of the fuel sag for a typical target of 1-mm diameter can be estimated as follows:

$$\tau_{gravity} \approx \sqrt{\frac{2R}{g}} \approx 10 \text{ ms},$$

where g is the free fall acceleration. In regard to the time of liquid phase existence $\tau_{lq} = \tau_4 - \tau_1$ it will suffice to monitor the value of $\tau_{3-1} = \tau_3 - \tau_1 < \tau_{lq}$. It is because of τ_{3-1} is only a part of the whole time interval τ_{lq} that it is actually a most convenient quantity to compare the calculation results. Herein after it is referred to as a "characteristic time" of liquid phase existence.

The left side of Table 1 shows the data for the glass shell. First, note that in the case of D_2 fuel τ_{3-1} is about 10 ms. The right side of Table 1 shows the data for the polystyrene shell. Since the heat capacity for polystyrene is less than for glass, then the value of τ_{3-1} should grow in magnitude. Our calculations show that even the value of $\tau_2 - \tau_1$ considerably exceeds 10 ms both for H_2 and D_2. Tables 2 and 3 present the results corresponding to variations in δR and $\tau_{surface}$. Evidently, the characteristic time τ_{3-1} grows with increasing in δR and $\tau_{surface}$.

Summarizing the obtained results, special attention should be given to the fact that in the most interesting case of polystyrene shell, the time of liquid phase existence exceeds 10 ms for thin shells, and 100 ms for thick shells. During this time, the liquid fuel will inevitably sag to the target bottom because, as estimated above, $\tau_{gravity} \approx 10$ ms.

Table 2. *The results obtained for the glass shell under variations in δR and $\tau_{surface}$*

$\tau_{surface}$	τ_1	τ_2	τ_3	τ_4
H_2 (25 mg/cc), $\delta R = 15$ μm				
1.0	5.83	10.74	15.59	18.71
10.0	25.93	35.81	42.23	47.07
H_2 (25 mg/cc), $\delta R = 25$ μm				
0.5	8.4	15.93	23.89	28.04
1.0	8.84	16.37	24.32	28.48
5.0	16.06	25.49	33.25	37.49
10.0	27.51	39.5	48.7	53.76

Thus, it is impossible to form a uniform cryogenic layer in the motionless target even in the case of high cooling rates. Below we consider the fuel formation in a moving target, namely: (a) due to its free fall in vacuum when it is cooled by radiative heat transfer only; and (b) due to the FST layering, or solid layer formation in a free-standing target moving in the layering channel (see Fig. 1), which allows the decrease of the effect of gravitational fuel sag, and, what is more important, the maintenance of rapid symmetrization mechanisms induced by target motion (see Sections 2.3 and 3).

2.2. Slow cooling rates; moving target

Under target cooling by radiative heat transfer only (free fall in vacuum), the external boundary condition is of the form

$$\left[4\pi r^2 k_{sh} \frac{\partial T_{sh}}{\partial r} + \sigma(T) \cdot T_{sh}^4\right]_{r=(1+\delta)R} = 0. \qquad (12)$$

The heat transport outside the shell is irradiation of a "black" or "gray" body. In this case, the rate of target cooling becomes negligible, and the layering time $\tau_{form} \propto \sigma$, where σ is the Stephen's constant. In other words, during the layering process in a free falling target, one can forget about the gravitational fuel sag and, as a consequence, form a per-

Table 3. *The results obtained for the polystyrene shell under variations in δR; H_2 (25 mg/cc), $\tau_{surface} = 1$ ms*

δR (μm)	τ_1	τ_2	τ_3	τ_4
1.0	7.99	16.90	30.13	38.04
1.5	11.39	24.00	44.20	54.89
2.0	15.04	31.17	58.47	71.88
3.0	23.01	45.89	87.86	106.57
5.0	41.67	77.87	150.22	179.19
10.0	95.62	168.2	327.86	382.47
15.0	189.31	293.89	538.04	617.96

https://doi.org/10.1017/S0263034602201020 Published online by Cambridge University Press

fectly uniform solid layer. However, in doing so, the layering time becomes experimentally unacceptable.

2.3. Moderate cooling rates; moving target or FST layering

The moderate cooling rates are realized when the target is cooled by heat conduction through a small contact area between the shell and the wall of the layering channel (see Fig. 1). For a given heat flux q at the external shell surface, one can write the following boundary condition:

$$\left[4\pi r^2 k_{sh}\frac{\partial T_{sh}}{\partial r}\right]_{r=(1+\delta)R} = -q. \quad (13)$$

Accounting for the heat removal in the contact area gives rise to another boundary condition, which holds true for thin shells:

$$[T_{sh}]_{r=(1+\delta)R} = (1-\chi)[T_{sh}]_{r=R} + \chi\cdot T_{external}. \quad (14)$$

The contact area occurs due to the shell deformation during its motion in the channel. In this case, the rate of heat transport outward from the target depends on the contact area size. Hence, there is a possibility to influence the time of condensed layer formation by varying the target trajectory or layering channel geometry. An estimation of the contact area as a function of the target parameters can be done from energy balance between the initial energy of the target center of mass and the energy of shell deformation. It is assumed that the spherical shape of the shell remains unchanged, excluding its bottom segment. This segment forms a circular area of contact. The elastic contraction of the shell material in this bottom segment consumes the initial energy of the target center of mass. The energy of the shell deformation W_{sh} and the occurring normal reaction of support are estimated in approximation of a thin shell. Assumption that the shell is thin is rather questionable in the case when shell displacement Δ is less then its thickness. Nevertheless, this estimation gives right insight to the problem. Table 4 summarizes the obtained results.

The following nomenclature is used: E is the Young's modulus, $\xi = \delta R/R$, V is the shell velocity, and C_s is the sound velocity, the parameter $\chi = r^2/4R^2$, where r is the contact area radius, r_{tube} is the layering channel radius.

Case A relates to a rolling target, which is always retained against a contact surface. The energy of the shell deformation corresponds to the work of the normal component N of the target pressure on the channel wall along the pass Δ. It can be, for example, the shell weight (formula A2 in Table 4), centrifugal force, and so forth. The force N exists quite long, but generates a comparatively small contact area.

Case B relates to a target trajectory, which has two alternative phases: the free-fall phase and the collision phase. The shell deformation occurs only during the second phase due to shell collision with the channel wall. The lifetime of the contact area is about $t \approx 2\Delta/V$. The shell deceleration occurring during collision phase $a \approx V^2/\Delta$ is considerably more than the free-fall acceleration g, and the impulsive braking force is considerably more than any feasible force N.

Thus, the target cooling is caused by heat conduction through either large, but short-lived contact areas (Case B), or small, but long-lived ones (Case A), which is characterized by a parameter $\epsilon = (2N\Delta/MV^2)^{0.5}$. For a typical target of 1-mm diameter, the estimations give $\chi \approx 10^{-4}$ (Case A) and $\chi \approx 10^{-3}$–10^{-4} at $V \geq 10$ cm/s (Case B). These estimations have demonstrated that the contact area size of $\chi \geq 10^{-4}$ can be formed under FST experimental conditions. Now let us show that the value of $\chi \geq 10^{-4}$ is quiet enough to form the cryogenic layer for several seconds. In this case the external boundary condition can be written in the form in which the heat flux at the outer shell surface becomes a parameter—Q (W/cm^2 K).

As for the temperature T_{in}, two remarks are in order. Since the heat capacity for polystyrene is less than for glass, then there is no sense to cool the target from $T_{in} = 300$ K. In addition, to fabricate the inner solid layer of ~ 100 μm in thickness, the shells are first filled to a pressure of $\sim$1000 atm at 300 K and then cooled down to a certain temperature T_d considerably less than 300 K. This is because of low strength and high permeability of hydrogen isotopes in polystyrene

Table 4. *Estimation of the contact area size*

Substrate	Case A: Rolling target		Case B: Colliding target	
Planar	$\chi \approx \sqrt{3W_{sh}/4pR^3E\cdot\xi}$	(A1)	$\chi \approx \sqrt{3M_{target}V^2/8pR^3E\cdot\xi}$	(B1)
	$\chi \approx \sqrt{\frac{3\cdot R\cdot g}{C_s^2}}$	(A2)	$\chi \approx \frac{V}{C_s}$, for an empty shell	(B2)
Cylindrical	$\chi \approx \sqrt{\frac{W_{sh}}{4pE\cdot R^3\cdot\xi}}\left(1+\frac{R}{r_{tube}}\cdot\frac{1}{4}-\frac{129}{32}\cdot\frac{R^2}{r_{tube}^2}\right)$		$\chi \approx \frac{V}{C_S}\cdot\frac{1}{\sqrt{2}}\left(1+\frac{R}{r_{tube}}\cdot\frac{1}{4}-\frac{129}{32}\cdot\frac{R^2}{r_{tube}^2}\right)$	

https://doi.org/10.1017/S0263034602201020 Published online by Cambridge University Press

Table 5. *The time moments of the onset and the end of fuel liquefaction and freezing for different values of Q and T_{in}*

Q	τ_1	τ_2	τ_2	τ_2
$T_{in} = 300$ K				
0.1	297.35	388.08	578.27	640.09
0.01	297.35	2657.75	3329.3	3459.91
$T_{in} = 36$ K				
2.0	13.54	91.67	274.07	337.85
0.1	18.7	109.61	299.77	31.48
0.01	70.51	432.3	1106.83	1234.02
0.002	292.34	2034.82	5253.67	6346.84

at room temperature (Aleksandrova & Belolipetskiy, 1999*a*, 1999*b*). The calculation results for different values of Q and T_{in} are given in Table 5 for a target ($R = 0.492$ μm and $\delta R = 0.01$ μm) filled with hydrogen H_2 (29 mg/cc, near critical point).

It is seen from Table 5 that $Q = 0.002$ (W/cm^2 K) gives a layering time of ≈6–7 s, which is in a good agreement with the FST experiments. On the other hand, it is evident that T_{in} becomes a parameter as well, and its choice cannot be independent.

Now determine the layering time as a function of the contact area size in the frame of one-dimensional model by changing the external boundary condition. This has been done numerically by solving Stephen's problem for moving boundaries between the fuel phases (gas, liquid, and solid) and for nonlinear boundary condition onto the outer shell surface.

Table 6 presents the comparative experimental and theoretical results. We use the following nomenclature: t_{res} is the target residence time in the layering channel, τ_{form} is the calculated layering time, and always $\tau_{form} \leq t_{res}$, NU_{in} and NU_{out} are the layer nonuniformity before and after target layering. In the FST experiments, several interchangeable layering channels: cylindrical (wide and narrow at vertically inclined geometry of the experiment) and spiral are used. The medium immediately surrounding the target inside the channel is vacuum or heat-exchanged helium at different pressures. Currently, the layered target is characterized conventionally using computer-aided CCD cameras

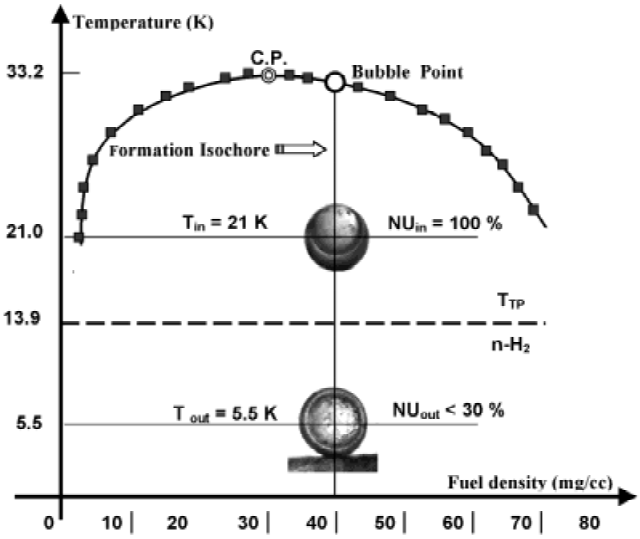

Fig. 2. A 88-μm-thick H_2 layer was formed in a cylindrical layering channel for a time of less than 8 s.

with one or two views. In the near future we plan to complete the FST system with a new characterization subsystem for tomographic target imaging (Aleksandrova *et al.*, 1999*b*, 2000*a*). Below we describe the conditions of FST experiments presented in Table 6 (Osipov *et al.*, 1999; Koresheva *et al.*, 2000; Aleksandrova *et al.*, 2000*b*):

- *Cylindrical channel with gaseous helium inside (line 2 in Table 6)*. A 983-μm-diameter polystyrene shell was filled up to 765 atm of H_2 at 300 K (gas density—40 mg/cc). The initial target temperature before layering was 21 K. According to the phase diagram (Fig. 2), the initial state of H_2 before layering was liquid + vapor with $NU = 100\%$. A 88-μm-thick layer with $NU < 30\%$ has been formed at 5.5 K inside the cylindrical channel (Figs. 2 and 3a). The layering time was no more than 8 s.
- *Spiral channel (line 4 in Table 6)*. A 980-μm-diameter polystyrene shell was filled up to 237 atm of D_2 at 300 K (gas density—33 mg/cc). The initial target temperature before layering was 26 K. According to the phase diagram, the initial state of D_2 before layering was liquid + vapor with $NU = 100\%$. A 30-μm-thick

Table 6. *The comparative experimental and theoretical results*

	Shell (polystyrene)							
Fuel	$2(R + \delta R)$ (μm)	δR (μm)	T_{in} (K)	W (μm)	t_{res} (s)	τ_{form} (s) at $\chi =$ 0.003–0.001	NU_{in} (%)	NU_{out} (%)
H_2^*	983	15	21	88	8	1–4	100	<30
H_2^*	983	15	15	88	8	0.3–1.4	100	100
D_2^{**}	980	20	26	30	12	2–6	100	<20

*cylindrical channel; **spiral channel.

https://doi.org/10.1017/S0263034602201020 Published online by Cambridge University Press

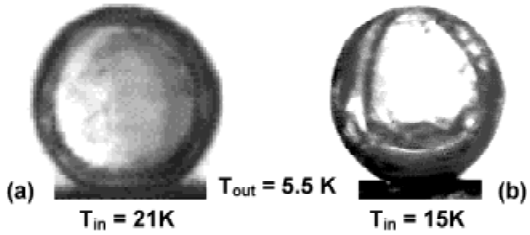

Fig. 3. Cryogenic layer formation at different initial temperatures.

layer with $NU < 20\%$ (which is a resolution limit for our current characterization system) has been formed at 5.5 K inside the spiral channel (Fig. 1). The layering time was no more than 12 s. Usage of the spiral layering channel allowed us to have a better uniformity of the layer.

Thus, according to FST layering experiments, both the channels provide a rapid self-symmetrization of a highly nonuniform liquid layer and formation of rather uniform solid layer (see Table 6, lines 2 and 4). The observed target residence time inside both layering channels and the calculated layering time are in a good agreement, and $\tau_{form} < t_{\rm res}$.

It should be noted that under lowering T_{in} to 15 K the symmetrization effect was not observed (see Table 6, line 3, and Fig. 3b). In the frame of our model, the following explanation can be proposed. Since the solid layer formation goes through the liquid phase, then the time of liquid phase existence is a key parameter and must be sufficient for layer symmetrization. At $T_{in} < 16$ K, this time is very small; at $T_{in} > 30$ K (bubble point), there is a gaseous fuel phase which requires some additional cooling time, which, in principle is a "dead layering time." Therefore, the temperature range of 16 K $< T_{in} < Ts$, where Ts is the initial temperature of fuel separation into liquid and gaseous phases, is the working range for the FST layering. Of course, the choice of an optimal T_{in} should be given for each particular formation isochore (see Fig. 2).

From physics, formation of a rather uniform solid layer directly from a highly nonuniform liquid layer can be controlled by a very simple mechanism. An "ice spot" is generated in the liquid phase (after its gravitational sag) in the vicinity of the contact area. Due to the target rolling along the layering channel, this ice spot is removed from the liquid, and the next one occurs in a new contact area between the shell and liquid layer. In doing so, the ice spot begins a random walk onto the inner shell surface, and the solid layer is formed similar to a thread applied onto a ball. In places of "ice outgrowths" arising, the heat removal becomes smaller and, as a result, the solid layer formation accelerates in the cavities and smooths them. For the described mechanism, the layer symmetrization time cannot exceed the layering time under conditions of $T_{in} = Ts$, and takes several seconds.

In the next section, we make an attempt to provide some grounding in theory for describing a more complex mechanism: initial symmetrization of the liquid layer with its further freezing resulting in a uniform solid layer. At present, this is an important aspect of our activity because the work in this direction can lead to a new, simpler construction of the layering channel. In essence, the generation of one or another mechanism depends on the target trajectory realized in the layering module, particularly, on the target velocity.

3. DYNAMICAL SELF-SYMMETRIZATION OF THE LAYER: SHALLOW WATER EQUATIONS FOR A ROLLING SPHERICAL TARGET

As the target is cooled, there comes a point where the fuel gas in the shell is all but liquefied. The life time of the liquid phase before the onset of fuel freezing considerably exceeds the time of gravitational sag $\tau_{gravity} \approx 10$ ms even in the case of high cooling rates (see Section 2). This means that the liquid fuel in a motionless target has the time to sag at the target bottom, which inhibits, or in more exact terms, makes impossible formation of a uniform cryogenic layer. The use of FST layering allows one to avoid the difficulties arising under solid layer formation in the motionless target. Below, a new mechanism is proposed for ICF target symmetrization to be successful. To withstand the gravitational fuel sag, the process of reaching the target symmetry goes in two stages: (1) rapid symmetrization of the liquid layer caused by a relatively high target velocity, and (2) further freezing of the symmetric liquid fuel resulting in a uniform solid layer.

Consider a rotating spherical target, which rolls down along the layering channel. The shell rotation causes a spread of liquid fuel over the inner shell surface. Under certain conditions it can result in a uniform layer formation. This important effect (refer it to as dynamical self-symmetrization) makes it topical to study a dynamical spread of the liquid fuel inside the moving target and to develop numerical models of the process. Therefore, we have initiated investigations in this field (Aleksandrova *et al*., 2001), and our first results are presented below.

Let a hollow spherical shell be partly filled with liquid fuel, and let us take H as a liquid layer thickness, which is $H/R \ll 1$ and $H/l \ll 1$, where l is a characteristic size of spatial nonuniformity of the layer. Since the liquid velocity is considerably less than the sound velocity in it, we can write 3D equations for incompressible liquid. Using conventional notations, they are of the form

$$\frac{\partial \vec{V}}{\partial t} + (\vec{V}\vec{\nabla})\vec{V} = -\frac{1}{\rho}\vec{\nabla}P - \vec{g}_{\otimes} + \nu\Delta\vec{V}, \tag{15}$$

$$\mathrm{div}\vec{V} = 0, \tag{16}$$

where $\vec{g}_{\otimes}$ is the liquid acceleration in a coordinate system connected with the target (system **T**). Equations (15) and (16) can be reduced to 2D shallow water equations onto a

https://doi.org/10.1017/S0263034602201020 Published online by Cambridge University Press

sphere. To do that, write the pressure across the layer in the form

$$P = \rho \cdot \left(\frac{U_\vartheta^2 + U_\varphi^2}{R} - g_\otimes \cdot \cos\vartheta \right) \cdot (r - R + H), \tag{17}$$

where r, ϑ, φ are the spherical coordinates in the system $\mathbf{T}$. By averaging ϑth and φth terms of Equation (15) over r and taking into account Equation (17), we have:

$$\frac{\partial U_\vartheta}{\partial t} + \frac{1}{R}\left(U_\vartheta \frac{\partial_\vartheta}{\partial\vartheta} + \frac{U_\varphi}{\sin\vartheta}\frac{\partial U_\vartheta}{\partial\varphi} - U_\varphi^2 \frac{\cos\vartheta}{\sin\vartheta} \right) = -\frac{1}{RH}\frac{\partial}{\partial\vartheta}\left(\left(\frac{U_\vartheta^2}{R} - g_\otimes \cdot \cos\vartheta \right) \frac{H^2}{2} \right) + g_\otimes \sin\vartheta + \frac{1}{\tau}(U_{0\vartheta} - U_\vartheta) + (viscosity)_\vartheta \tag{18a}$$

$$(viscosity)_\vartheta \equiv \frac{\nu}{R^2 \sin^2\vartheta} \times \left(\sin\vartheta \frac{\partial}{\partial\vartheta}\left(\sin\vartheta \frac{\partial U_\vartheta}{\partial\vartheta} \right) + \frac{\partial^2 U_\vartheta}{\partial\varphi^2} - U_\vartheta - 2\cos\vartheta \frac{\partial U_\varphi}{\partial\varphi} \right) \tag{18b}$$

$$\frac{\partial U_\varphi}{\partial t} + \frac{1}{R}\left(U_\vartheta \frac{\partial U_\varphi}{\partial\vartheta} + \frac{U_\varphi}{\sin\vartheta}\frac{\partial U_\varphi}{\partial\varphi} + U_\varphi U_\vartheta \frac{\cos\vartheta}{\sin\vartheta} \right) = -\frac{1}{\sin\vartheta}\frac{1}{RH}\frac{\partial}{\partial\varphi}\left(\left(\frac{U_\vartheta^2 + U_\varphi^2}{R} - g_\otimes \cdot \cos\vartheta \right) \frac{H^2}{2} \right) + \frac{1}{\tau}(U_{0\varphi} - U_\varphi) + (viscosity)_\varphi \tag{19a}$$

$$(viscosity)_\varphi \equiv \frac{\nu}{R^2 \sin^2\vartheta} \times \left(\sin\vartheta \frac{\partial}{\partial\vartheta}\left(\sin\vartheta \frac{\partial U_\varphi}{\partial\vartheta} \right) + \frac{\partial^2 U_\varphi}{\partial\varphi^2} - U_\phi + 2\cos\vartheta \frac{\partial U_\vartheta}{\partial\varphi} \right). \tag{19b}$$

Here τ is the time of engagement between $\vec{U}$ and $\vec{U}_0$. Equations (18) and (19) should be added with an equation for layer thickness:

$$\frac{\partial H}{\partial t} + \frac{1}{R\sin\vartheta}\left(\frac{\partial}{\partial\vartheta}(U_\vartheta H \sin\vartheta) + \frac{\partial(U_\varphi H)}{2\varphi} \right) = 0. \tag{20}$$

Our analysis shows that one can expect the layer symmetrization only if the vector of instantaneous angular velocity $\vec{\Omega}(t)$ in (18) and (19) is time and space dependent (effect of rotation axis wobble):

$$\begin{aligned} \Omega_x &= \Omega(t) \cdot \sin\Theta \cdot \cos\Phi \\ \Omega_y &= \Omega(t) \cdot \sin\Theta \cdot \sin\Phi \\ \Omega_z &= \Omega(t) \cdot \cos\Theta, \end{aligned} \tag{21}$$

where $\Theta(t), \Phi(t)$ are the spherical angles of the vector $\vec{\Omega}(t)$. Since the rotation velocity in the system $\mathbf{T}$ is $\vec{U}_0 = -[\vec{R} \times \vec{\Omega}]$, then the spherical velocity components of the rolling target in (18) and (19) are:

$$\begin{aligned} U_{0r} &\equiv 0 \\ U_{0\vartheta} &= -R\Omega \cdot (\sin\Theta \cdot \sin(\varphi - \Phi)) \\ U_{0\varphi} &= -R\Omega \cdot ((-\sin\vartheta \cos\Theta + \sin\Theta \cos(\varphi - \Phi)\cos\vartheta)). \end{aligned} \tag{22}$$

Equations (18)–(22) can be integrated numerically which allows us to make a conclusion about layer symmetrization by varying the Reynolds number, the parameters of engagement (τ) and rotation ($\vec{\Omega}$).

Further we estimate a role of the effect of rotation axis wobble. Suppose that the liquid velocity practically coincides with the shell velocity. Then, the square of the liquid layer velocity which enters in the layer pressure onto the shell is equal to

$$U_{0\vartheta}^2 + U_{0\varphi}^2 = R^2\Omega^2 \cdot (\sin^2\vartheta \cos^2\Theta - \tfrac{1}{2}\sin 2\vartheta \cdot \sin 2\Theta \cdot \cos(\varphi - \Phi) + \sin^2\Theta \cdot (\sin^2(\varphi - \Phi) + \cos^2(\varphi - \Phi) \cdot \cos^2\vartheta)). \tag{23}$$

Now, let us average this expression over the time, taking that the amplitude of the angular velocity Ω is constant, but the angles Θ and Φ are not correlated and change randomly near their mean values

$$\Theta = \frac{\pi}{2} + \xi \cdot W_1(t) \qquad \text{and} \qquad \Phi = \eta \cdot W_2(t), \tag{24}$$

where $W_1(t)$ and $W_2(t)$ are randomly chosen in the range $[-1,1]$, and ξ, η are the numerical coefficients (they are ≤ 1). After averaging we have

$$\langle U_{0\vartheta}^2 + U_{0\varphi}^2 \rangle = R^2\Omega^2 \cdot (\sin^2\vartheta \langle \cos^2\Theta \rangle + \langle \sin^2\Theta \rangle \cdot (\langle \sin^2(\varphi - \Phi) \rangle + \langle \cos^2(\varphi - \Phi) \rangle \cdot \cos^2\vartheta)).$$

https://doi.org/10.1017/S0263034602201020 Published online by Cambridge University Press

In particular, at $\varphi = 0$,

$$\langle U_{0,\vartheta}^2 + U_{0\varphi}^2 \rangle = R^2\Omega^2 \cdot \left(\frac{\xi^2}{3} \sin^2 \vartheta + \cos^2 \vartheta + \frac{\eta^2}{3} \right), \quad (25)$$

so that the layer nonuniformity along the shell can be estimated as

$$\left(0 \le \vartheta \le \frac{\pi}{2}\right):$$

$$H^2 \cdot \left(R\Omega^2 \cdot \left(\cos^2 \vartheta + \frac{\xi^2}{3} \sin^2 \vartheta + \frac{\eta^2}{3} \right) - g_{\otimes} \cos \vartheta \right)$$

$$\approx const. \quad (26)$$

This means that $NU \sim 10\%$ and less can be reached at

$$\frac{(\xi^2 + \eta^2)}{3} \le 1 + \frac{\eta^2}{3} - \frac{g_{\otimes}}{R\Omega^2} \le 1.1 \cdot \frac{(\xi^2 + \eta^2)}{3}. \quad (27)$$

The last expression indicates a range (rather narrow) for changing a "rolling" parameter $g_{\otimes}/R\Omega^2$:

$$\left(1 - \frac{\xi^2}{3}\right) - 0.1 \cdot \frac{\xi^2 + \eta^2)}{3} \le \frac{g_{\otimes}}{R\Omega^2} \le \left(1 - \frac{\xi^2}{3}\right). \quad (28)$$

Summarizing this section, two remarks should be made. First, in the opposite case of steady-state rotation, the layer thickness by rough estimation is $H \approx const \cdot (\cos \vartheta)^{-1}$, and no layer symmetrization can be expected. Second, experimentally, the behavior of $\vec{\Omega}(t)$ in time can differ from that described above. But it was important to show that just rotation axis wobble can significantly influence the liquid layer symmetrization. This process appears to have considerable promise for development of new layering module designs, for example, a shaker-like unit. Such a layering module can hold a large number of targets (more than 500) and work with them at one time. Because the layering time is short enough, only tens of seconds, the above proposal can be considered as a new FST scenario for mass-producing the cryogenic targets.

4. FUTURE TRENDS OF DEVELOPMENT

In this work, we have discussed the theory, simulation program, numerical, and experimental results for FST layering, including the detailed descriptions of the heat transfer and layer symmetrization mechanisms. Formation of a solid layer is analyzed for targets moving in the layering module. The aim of these targets is to demonstrate large benefits of a layering—*plus*—delivery scheme for rep-rate cryogenic target fabrication. Currently, the FST system operates with 25 targets at one time. The targets move downward along the layering module in a rapid succession—one after another, which results in a repetitive target injection into the test chamber (see Fig. 1). This allows shortening the layering time per target. An experimental study of the target injection system in a rep-rate regime of six targets each second is underway.

The proposed FST model can be adaptable and scalable for the rep-rate fabrication of large cryogenic targets both for new megajoule-class laser facilities and inertial fusion energy power plant.

5. CONCLUSION

In ICF research, considerable recent attention has been focused on the issue of cryogenic target fabrication for a high-energy laser driver. Analyzing the obtained results, we can conclude that the FST layering is a suitable candidate to meet the goal. The experience thus far gained for solving the issues on filling, layering, and delivering large, free-standing, cryogenic targets is sufficient to elaborate a special R&D program that is directed to target factory creation. A broad program for reactor-scaled target fabrication and delivery at the center of the target chamber was set up at LPI in 2000.

REFERENCES

Aleksandrova, I.V. & Belolipetskiy, A.A. (1999*a*). An efficient method for filling targets with a highly-pressurized gas fuel. *J. Moscow Phys. Soc.* **9**, 325–337.

Aleksandrova, I.V. & Belolipetskiy, A.A. (1999*b*). Mathematical models for filling polymer shells with a real-gas fuel. *Laser Part. Beams* **17(4)**, 701–712.

Aleksandrova, I.V., Belolipetskiy, A.A., Golov, V.I., Chtcherbakov, V.I., Makeyeva, E.V., Koresheva, E.R. & Osipov, I.E. (2000*a*). Progress in the development of tomographic information processing methods for applications to ICF target characterization. *Fusion Technol.* **38(2)**, 190–205.

Aleksandrova, I.V., Chtcherbakov, V.I. & Bazdenkov, S.V. (2001). Rapid fuel layering inside moving free-standing ICF targets: Physical model and simulation code development. *Proceedings of SPIE* **4424**, 197–205.

Aleksandrova, I.V., Koresheva, E.R., Krokhin, O.N. & Osipov, I.E. (1999*a*). Statistical investigations of cryogenic target formation and future trends of development. *J. Moscow Phys. Soc.* **9**, 311–324.

Aleksandrova, I.V., Koresheva, E.R. & Osipov, I.E. (1993). The changes in the morphology of frozen hydrogen izotope layers under the target heating. *J. Moscow Phys. Soc.* **3(2)**, 85–100.

Aleksandrova, I.V., Koresheva E.R. & Osipov, I.E. (1994). ICF cryotargets: Science and technology. *J. Moscow Phys. Soc.* **4(2)**, 81–128.

Aleksandrova, I.V., Koresheva E.R. & Osipov, I.E. (1996*a*). Injection as a principle of the target transport among the basic units: Fill system—layering module—target chamber. *Preprint LPI.* **34**, 25p.

Aleksandrova, I.V., Koresheva, E.R. & Osipov, I.E. (1999*b*). Free-standing targets for applications to ICF. *Laser Part. Beams* **17(4)**, 713–727.

Aleksandrova, I.V., Koresheva, E.R., Osipov, I.E. & Panina, L.V. (1996*b*). Cryotargets for modern ICF experiments. *Laser Part. Beams* **6(2)**, 539–551.

https://doi.org/10.1017/S0263034602201020 Published online by Cambridge University Press

Aleksandrova, I.V., Koresheva, E.R., Osipov, I.E., Tolokonnikov, S.M., Rivkis, L.A., Baranov, G.D., Veselov, V.P. & Yaguzinskiy, L.S. (2000*b*). Free-standing target technologies for ICF. *Fusion Technol.* **38(1)**, 166–172.

Koresheva, E.R., Aleksandrova, I.V., Baranov, G.D., Beloplipetskiy, A.A., Veselov, V.P., Listratov, V.I., Osipov, I.E., Rivkis, L.A., Soloviev, V.G., Timofeev, I.D., Tolokonnikov, S.M., Usachev, G.S. & Yaguzinskiy, L.S. (2000). Current results in the area of cryogenic fuel layering obtained at realization of the ISTC project #512. In: *Inertial Fusion Science and Application 99*, pp. 897–902. Paris: Elsevier.

Koresheva, E.R., Osipov, E.E. & Aleksandrova, I.V. (1994). ICF cryotargets: Delivery. *J. Moscow Phys. Soc.* **4(3)**, 183–242.

Osipov, I.E., Koresheva, E.R. & Baranov, G.D. (1999). A ramp-filling procedure applied to filling polymer and glass shell with highly pressurized hydrogens. *J. Moscow Phys. Soc.* **9**, 301–309.

https://doi.org/10.1017/S0263034602201020 Published online by Cambridge University Press